Eur. Phys. J. B **4**, 369–377 (1998)

THE EUROPEAN PHYSICAL JOURNAL B

I. Formation and rise of a bubble stream in a viscous liquid

P. Snabre[a] and F. Magnifotcham

Institut de Science et de génie des matériaux et procédés[b], BP5, 66125 Font-Romeu, France

Received: 23 July 1997 / Revised: 16 December 1997 / Accepted: 11 May 1998

Abstract. The continuous emission of gas bubbles from a single ejection orifice immersed in a viscous fluid is considered. We first present a semi empirical model of spherical bubble growth under constant flow conditions to predict the bubble volume at the detachment stage. In a second part, we propose a physical model to describe the rise velocity of in-line interacting bubbles and we derive an expression for the net viscous force acting on the surrounding fluid. Experimental results for air/water-glycerol systems are presented for a wide range of fluid viscosity (43 mPa s − 800 mPa s) and compared with theoretical predictions. An imagery technique was used to determine the bubble size and rise velocity. The effects of fluid viscosity, gas flow rate, orifice diameter and liquid depth on the bubble stream dynamic were analyzed. We have further studied the effect of large scale recirculation flow and the influence of a neighbouring bubble stream on the bubble growth and rising velocity.

PACS. 47.55-t Nonhomogeneous flows – 47.55.Dz Drops and bubbles – 47.10.+g General theory

1 Introduction

Bubbles play a significant role in many important industrial processes. Air bubblers are used in biochemical, polymer and other industries for improving the heat and mass transfer from a dispersed gaseous phase to the viscous liquid phase. In glass tank furnaces, rows of bubbles generated in vertical streams reinforce glass currents, insure glass uniformity and improve fining [1]. In many of these processes, bubbles are formed by blowing a constant gas flow through a fine capillary tube immersed in the fluid phase.

The present paper concerns the bubble formation in a quiescent liquid and the momentum exchange between a vertically upward stream of in-line interacting bubbles and the surrounding fluid. The process of bubble growth is of great influence on the bubble volume and rise velocity. Many workers have investigated the dynamic of bubble growth from immersed orifices in Newtonian fluids and a review has been published by Kumar and Kulor [2]. In a first section, we present a semi empirical model of bubble growth based on a dynamic force balance [2–8]. After the detachment stage, the bubble rising velocity depends on buoyancy forces and hydrodynamic interactions. The problem of in-line interacting bubbles has received much less attention. In the present work, we propose both an analogy with the settling of cylinders and a mean field model based on the estimation of the energy dissipation in the fluid phase to estimate the upward velocity rise of the bubble chain and the viscous force acting on the fluid. In a second section, we present experiments with water-glycerol solutions for a wide range of fluid viscosity (43 mPa s – 800 mPa s), air flow rate up to 0.5 l/mn and nozzle orifice diameter from 0.3 mm to 0.6 mm. From visualization and sequential image acquisition, we determine both the volume and the velocity rise of bubbles generated in a stream. In the last section, we discuss the effect of large scale recirculation flow and the influence of a neighbouring bubble stream on the process of bubble formation. The objectives of the present work were to develop a physical analysis of the bubble stream dynamics in a viscous fluid and to compare the predictions of the model with the experimental investigation. The companion paper concerns the experimental and numerical study of the recirculation flow induced by a rising chain of bubbles in a tank [30].

2 Bubble formation in a viscous liquid

A schematic diagram of the ideal formation of spherical bubbles is shown in Figure 1. We consider a long vertical capillary tube (inner diameter d_a) submerged in a viscous fluid (viscosity η , density ρ). Gas flowing (density ρ_g) at constant flow rate Q through the tube causes the formation of a bubble until detachment from the nozzle. The use of a long capillary tube insures the gas flow rate to be constant during bubble growth. The periodic emission of bubbles then results in a vertical rising bubble stream. The liquid is deep compared to the bubble diameter and the liquid bath is large so that the effect of both side walls and large scale recirculation flow are negligible.

[a] e-mail: snabre@imp-odeillo.fr

[b] UPR 8521.

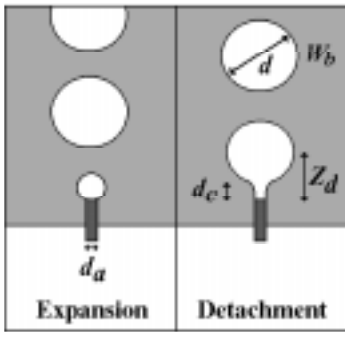

Fig. 1. Schematic representation of bubble stream formation.

For low values of the Reynolds number ($Re = Wd\rho/\eta < 1$ where g is the gravity acceleration, d the bubble diameter and W the bubble average velocity) one can consider a spherical growth of bubbles [9]. Direct observations by high speed cinematography show two stages in the bubble formation at constant gas flow [2,8]. During the expansion stage, the bubble remains attached to the nozzle tip and the diameter d of the spherical drop (volume $V = \pi d^3/6$) increases with time. At the beginning of the detachment stage, the net upward force becomes greater than the downward force. The spherical bubble then moves away from the orifice but remains connected to the nozzle through a cylindrical neck (Fig. 1). In most of the theoretical studies [2–8] the bubble volume is derived from a semi empirical model based on a force balance around the spherical bubble at the instant just previous to detachment when the neck is broken off:

$$F_b + F_g + F_p = F_d + F_i + F_\sigma \tag{1}$$

- buoyancy force $F_b = (\rho - \rho_g)gV$
- gas momentum force $F_g = \frac{\pi}{4} d_a^2 \rho_g W_g^2$ with $W_g = 4Q/(\pi d_a^2)$
- pressure force $F_p = \frac{\pi}{4} d_a^2 (P_g - P)$
- drag force $F_d = \frac{1}{2}\rho W^2 \frac{\pi d^2}{4} C_d^*$
- inertial force $F_i = \left(\alpha + \frac{\rho_g}{\rho}\right)\rho V\gamma$
- surface tension force $F_\sigma = \pi d_a \sigma$

where W_g is the gas velocity through the tube, W the average velocity of bubble expansion, γ the average bubble acceleration, C_d^* the average drag coefficient, σ the surface tension of the liquid, P_g the gas pressure in the bubble and P the average liquid pressure.

We can neglect the pressure force acting in the upward direction since the gas pressure P_g in the bubble is equal to the liquid pressure at the plane of the bubble base. The inertial force associated to the momentum of the surrounding liquid motion involves an added fluid mass $\alpha\rho V$ considered at the point of detachment. Nozzle wall effects may influence the dimensionless inertial parameter $1/2 \leq \alpha \leq 11/16$ since the added mass is $\rho V/2$ for a sphere in an infinite stream and $11\rho V/16$ for a sphere moving perpendicular to a wall in inviscid fluid [10].

Convective or recirculation flows may have some influence on the growth process and the bubble size at the detachment stage [8–11]. Chuang and Goldschmidt [12] have proposed a first order expression of the modified drag force F_d acting on a bubble in upward flow (average velocity U) based on the relative co-flowing velocity $U - W$:

$$F_d = C_d^* \frac{\pi}{4}(d^2 - d_a^2)(U - W)^2 \frac{\rho}{2} \cdot \tag{2}$$

If bubbles are generated in a stream with a high frequency, the bubble may further experience an additional upward force due to the wake formed by the preceding bubble. Experiments from Chuang and Goldsmith only show a wake effect for closely interacting bubbles generated from small capillaries ($d_a < 100$ μm) with a high frequency emission [12].

In the present work, we consider moderate gas flow rate and we neglect both gas momentum ($\rho_g \ll \rho$), wake effects and recirculation flows near the nozzle ($U \ll W$). The force balance (1) at the moment of bubble detachment then becomes:

$$\rho g V = \frac{\pi}{8} d^2 C_d^* \rho W^2 + \pi d_a \sigma + \alpha \rho V \gamma \cdot \tag{3}$$

The average expansion velocity W and average acceleration γ must now be defined. In the detachment stage, the bubble base begins to rise vertically until the bubble neck breaks off. Most of the models use an empirical relation for the distance Z_d covered by the bubble centre at the end of the detachment stage (Fig. 1). The analysis of cine-photographs indicates that the length d_c of the bubble neck just prior detachment lies in the range $0 < d_c < d/2$ [2,5,13]. Therefore, we assume a length neck $d_c \approx d/4$ in good agreement with accurate measurements made by Räbiger *et al.* [14]. From the bubble expansion time $t_b = V/Q$ and the translation distance $Z_d \approx d/2 + d_c \approx 3d/4$ of the bubble centre at the detachment stage, a first order approximation of the bubble average expansion velocity W and bubble average acceleration γ is derived:

$$W \approx \frac{Z_d}{t_b} = \frac{3dQ}{4V} \quad \text{and} \quad \gamma \simeq \frac{W}{t_b} = \frac{WQ}{V} \cdot \tag{4}$$

Substituting the above relations in the force balance (3), we get :

$$\frac{\pi}{3} d^3 \rho g = \left(\frac{81 C_d^*}{16} + 9\alpha\right) \frac{\rho Q^2}{\pi d^2} + \pi d_a \sigma \cdot \tag{5}$$

Several analytical forms of the drag coefficient for a freely rising bubble are available [2,13]. Experimental data from Miyahara *et al.* [15,16] and Al Hayes [17] give a drag coefficient $C_d = 16/Re + 1$ close to unity for large Reynolds number (Fig. 2). Since the growing bubble is attached to the nozzle, most of authors assume no internal gas circulation at low Reynolds number and then use the Stokes relation $C_d^* = 24/Re$ for a solid sphere [2]. Despite the bubble attachment which limits the internal gas circulation, large growing bubbles are expected to behave differently from

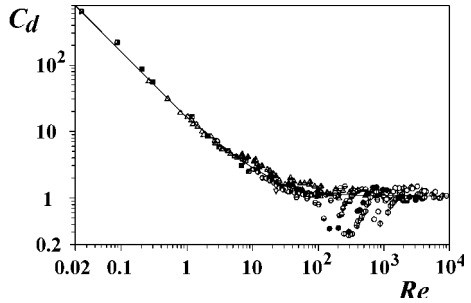

Fig. 2. Drag coefficient $C_d(Re)$ of single air bubbles freely rising in various liquids from Miyahara and Takahashi [15]. For Morton number $M = g\eta^4/(\rho\sigma)^3 > 10^{-7}$, experimental data are well represented by $C_d = 16/Re + 1$ (solid line).

solid spheres at high Reynolds number. Therefore, we consider a solid sphere behavior in the creeping regime and a freely circulating sphere in the inertial regime to derive a semi empirical formula for the drag coefficient C_d^* of a growing bubble over the whole Reynolds number range:

$$C_d^* = \frac{24}{Re} + 1 \quad \text{with} \quad Re = \frac{\rho W d}{\eta} \cdot \tag{6}$$

The bubble detachment diameter given by the force balance (5) then depends on gas flow rate, fluid viscosity, fluid density, surface tension and orifice diameter.

Surface tension forces only play a significant role at low gas flow rates [7]. The bubble diameter then becomes very sensitive to nozzle geometry and convective flows.

For high fluid viscosity and intermediate gas flow rates, one can neglect inertial and surface tension forces so that the bubble size mainly results from the balance between the downward drag force and the upward buoyancy force. The bubble diameter at low Reynolds number then scales as $[Q^2/(gRe)]^{1/5}$.

Under high gas flow rate and high pressure conditions, the gas momentum force is observed to have a great influence on bubble formation [6,7]. In the inertial regime ($Re \gg 1$), the force balance (5) gives a bubble diameter $d \approx [\alpha Q^2/g]^{1/5}$ involving the dimensionless inertial parameter α.

3 Rising velocity of bubble streams

This section concerns the velocity rise of in-line interacting bubbles generated in a stream. The problem of the free velocity rise W_0 of a single bubble in creeping flow was solved independently by Hadamard [18] and Rybczynski [19] from the Stokes stream functions for the outer and inner fluids:

$$W_0^2 = \frac{4}{3}\frac{d(\rho - \rho_g)g}{\rho C_d} \quad \text{with} \quad C_d = \frac{8}{Re}\frac{3\chi + 2}{\chi + 1} \tag{7}$$

where χ is the ratio of gas to liquid viscosity and the expression of the drag coefficient $C_d(\chi, Re)$ accounts for bubble internal circulation in viscous liquids. For a gas phase of weak viscosity and density ($\chi \approx 0$ and $\rho_g \ll \rho$), the bubble rising velocity in an unbounded viscous fluid then obeys:

$$W_0^2 = \frac{4}{3}\frac{dg}{C_d} \quad \text{with} \quad C_d = \frac{16}{Re} \cdot \tag{8}$$

Experiments by Miyahara *et al.* [16] for single bubble freely rising through high viscosity glycerol – water or glycerol – ethanol solutions give a drag coefficient $C_d = 16/Re + 1$ close to unity for Reynolds number $Re > 30$ (Fig. 2).

For bubbles generated in a stream, in-line hydrodynamic interactions and wake effects influence the bubble velocity rise. Hydrodynamic models of bubble streams are either empirical [20] or limited to pair-interacting bubbles [21–24]. Two identical spherical bubbles rise more rapidly than a single bubble when separated by a critical distance [21–23].

We first develop a physical approach based on the analogy with the sedimentation at low Reynolds number of a long cylinder in an unbounded viscous fluid. The free settling velocity $W_\perp$ of a long cylinder moving perpendicularly to the symmetry axis is half the velocity $W_\parallel$ of the cylinder with the main axis parallel to the flow direction [25]. The reduced viscous resistance of a cylinder aligned in the flow arises from the decrease in the drag coefficient.

In the case of a vertical bubble sream rising with a stationnary velocity W_b, we introduce the gas volume fraction $\varepsilon = Qd/(W_b V)$ in the gas-liquid column. A linear interpolation of the inverse drag coefficient $1/C_i$ between the limit values $1/C_i(\varepsilon = 0) = 1/C_d$ for isolated bubbles and $1/C_i(\varepsilon = 1) = 2/C_d$ for closely in-line interacting bubbles then gives a first order approximation of the drag coefficient $C_i(\varepsilon)$ for a vertical bubble stream:

$$\frac{1}{C_i(\varepsilon)} = \frac{1 + \varepsilon}{C_d} \cdot \tag{9}$$

Substituting the above drag coefficient in equation (8) yields the rise velocity $W_b(\varepsilon)$ of in-line interacting bubbles:

$$W_b^2 = \frac{2dg(1 + \varepsilon)}{C_d} = W_0^2(1 + \varepsilon) \quad \text{with} \quad \varepsilon = \frac{Qd}{W_b V} \cdot \tag{10}$$

We may also develop a mean field theory based on the estimation of the viscous dissipation in the liquid phase to estimate the gas volume fraction dependence of the bubble stream rise velocity. Similar energetic models were used to predict the viscosity of suspension or the sedimentation velocity of particles in concentrated systems [26,27].

At low Reynolds number, the change in potential energy associated to a steady flow is balanced by the viscous dissipation in the fluid. The volumetric change in potential energy per unit time is the product of the bubble rise velocity W_b and the vertical mean pressure gradient $\langle \nabla P \rangle = (\rho - \rho_g)g\varepsilon$ along the vertical gas-liquid column.

The change in potential energy E_p per unit time during the rise of a bubble stream of height H then takes the form:

$$E_p = \langle \nabla P \rangle W_b H \frac{\pi d^2}{4} \approx \rho g \varepsilon W_b H \frac{\pi d^2}{4} \cdot \quad (11)$$

The viscous dissipation per unit volume and unit time is a quadratic function of the shear gradients in the liquid phase. Neglecting the viscous dissipation in the liquid volume trapped between bubbles and assuming a flow perturbation over a distance of about the bubble diameter, the time rate of change of the viscous dissipation E_V along the bubble column may be approximated as:

$$E_V \approx \eta \left(\frac{W_b}{d}\right)^2 \left(\frac{9\pi d^2}{4} - \frac{\pi d^2}{4}\right) H \cdot \quad (12)$$

The condition $E_p = E_V$ then gives a linear dependence of the quadratic bubble velocity with the gas volume fraction in the stream in agreement with equation (10):

$$W_b^2 \approx dg\varepsilon \frac{d\rho W_b}{8\mu} \approx \frac{2dg}{C_d}\varepsilon \quad \text{with} \quad C_d = \frac{16}{Re} \cdot \quad (13)$$

However, the above relation fails to describe the motion of a single bubble ($\varepsilon \to 0$) since the expression of the viscous dissipation E_V is valid only for closely interacting bubbles. In the next section, the velocity rise of a bubble stream is derived from the non linear equation $W_b^2 = 2gd(1+\varepsilon)/C_d$ with $\varepsilon = Qd/W_b V$ and $C_d = 16/Re + 1$.

4 Average bubbling force

The rising chain of bubbles acts as an exterior shear force on the surrounding fluid and thereby induces a forced convection flow of the liquid phase. The coupling between the rising bubble stream and the surrounding liquid may be introduced into the momentum conservation equation of the liquid phase through a source term equals to the average bubbling force per unit volume acting on the gas in the bubble stream [30].

Neglecting bubble acceleration after detachment and the deceleration stage near the liquid free surface, we assume a uniform rise velocity $W_b(\varepsilon)$ of bubbles generated in a stream.

The change of the potential energy along the rising bubble column is then balanced by the work $E_b = F_b W_b$ of the net average bubbling force. The condition $E_b = E_p$ together with equation (11) then gives the net average bubbling force:

$$F_b = \frac{\pi d^2 H}{4} \rho g \varepsilon \cdot \quad (14)$$

By introducing the number $N = \varepsilon(\pi d^2/4)H/V$ of bubbles in the gas-liquid column, the net average bubbling force F_b then simply reduces to the buoyancy force acting on the gas in the bubble stream:

$$F_b = \rho g N V \cdot \quad (15)$$

The vertical average buoyancy force per unit volume $S_{bz} = \rho g \varepsilon$ appears in the momentum equations of the liquid phase as a source term which only acts over the gas-liquid column and induces a large scale recirculation flow [30].

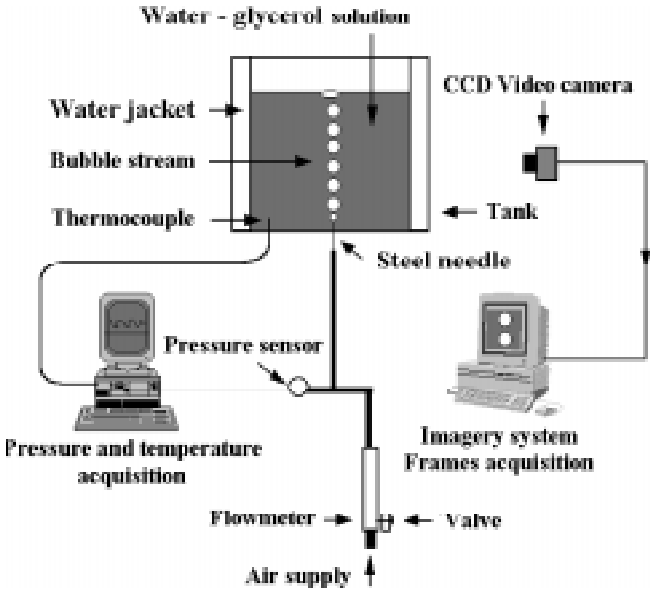

Fig. 3. Schematic diagram of the experimental set-up.

5 Experiments

A schematic diagram of the experimental set up is shown schematically in Figure 3. The experiments were performed in a glass tank of 20 cm × 20 cm cross-section and 20 cm height. The tank was filled with a Newtonian water-glycerol solution of viscosity in the range from 43 mPa s up to 800 mPa s and density 1200 kg/m^3 $< \rho <$ 1260 kg/m^3. A Couette rheometer (Low shear 30, Contraves) was used to measure the viscosity of water-glycerol solutions. The liquid temperature was maintained to 20 °C with a water jacket surrounding the tank and controlled with ± 0.1 °C accuracy. Water concentration weakly influences the surface tension $\sigma \approx 0.06$ N/m of aqueous glycerol solutions in air [4,15,29]. The bubbles were formed by blowing air at constant flow rate through a steel tube (10 cm length, inner diameter $d_a = 0.3$ mm, 0.4 mm or 0.6 mm). The emission orifice was submerged in the viscous fluid (liquid depth 5 cm $< H <$ 12 cm) at some millimetres from the bottom wall. A steady gas flow rate up to 0.5 l/mn was established and measured with flowmeters of different ranges (0.01 l/mn - 0.1 l/mn, 0.05 l/mn - 0.5 l/mn) calibrated with a rotameter. The bubble frequency emission ω was determined from the fast Fourier transform of the periodic signal from a differential pressure transducer (Sedeme Kistler, 0-20 mbar) since the gas pressure

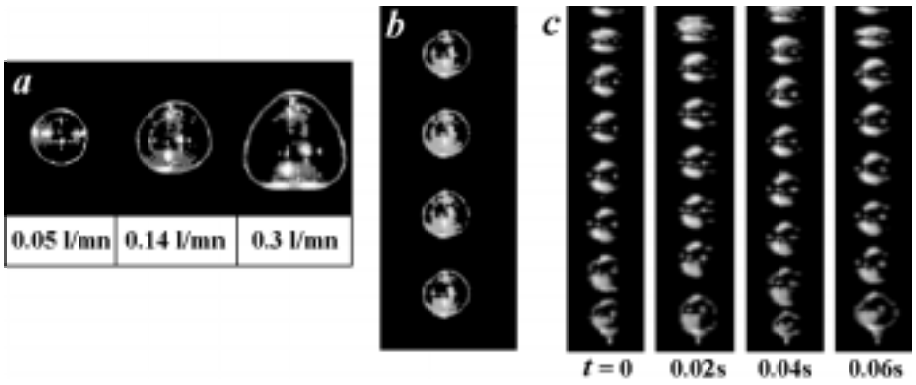

Fig. 4. Bubble formation in water-glycerol solution for nozzle diameter $d_a = 0.6$ mm. a) Bubble visualization at air flow rate $Q = 0.048$ l/mn, $Q = 0.14$ l/mn and $Q = 0.3$ l/mn ($\eta = 164$ mPa s), b) bubble stream ($Q = 0.048$ l/mn, $\eta = 105$ mPa s). c) Succession of images recorded at time $t = 0$ s, 0.2 s, 0.4 s and 0.6 s at the video frequency 50 Hz ($Q = 0.08$ l/mn, $\eta = 800$ mPa s).

changes around the average value $\langle P_0 \rangle = \rho g H$ are related to the bubble formation sequence.

The rising bubble stream was analyzed using a 512 × 512 pixel resolution CCD camera (Sony XC77RR) with 256 grey level resolution. The CCD camera operates in conjunction with a Mattrox PIP 1024 imaging unit and a PC compatible for the digitisation and storage of image data. The calibration factor for the field of view and any magnification was measured prior to frame record. A succession of 4 frames was then recorded at 50 Hz video frequency in non interlaced mode for a better contrast (time interval between frames 0.02 s, Fig. 4c). Specific numerical algorithms were developed to determine the average bubble size and rise velocity with 2% accuracy in successive image frames. We consider the equatorial diameter a and the height b of the bubble to estimate the bubble volume $V = 4\pi a^2 b/3$ and account for small bubble deformation from the spherical shape at high gas flow rates (Fig. 4a).

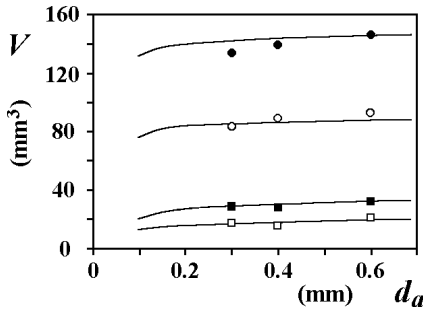

Fig. 5. Bubble volume V *versus* orifice diameter d_a. Experimental results for liquid viscosity $\eta = 43$ mPa s ($Q = 0.03$ l/mn (□), $Q = 0.06$ l/mn (■)) and $\eta = 800$ mPa s ($Q = 0.03$ l/mn (○), $Q = 0.06$ l/mn (●)). Solid lines are calculated from equation (5) with $C_d^* = 24/Re + 1, \alpha = 11/16$ and $\sigma = 0.06$ N/m.

5.1 Bubble volume and bubble frequency emission

Bubbles generated in a stream are uniform in size (Fig. 4b). The gas volume fraction $\varepsilon = NV/(\pi d^2 H/4)$ in the bubble stream ranges from 0.15 up to 0.55 at high gas flow rates. In the stable bubbling regime, the separation distance between bubbles always exceeds a value $\approx 0.7d$ for gas flow rates $Q < 0.5$ l/mn and therefore we may neglect wake effects during bubble growth.

In the low flow rate regime ($Q < 0.02$ l/mn), bubble formation is surface tension controlled since inertia and viscous forces are negligible compared to surface tension forces. The bubble diameter is then very sensitive to the nozzle diameter.

Under higher gas flow rates conditions ($Q > 0.05$ l/mn), either viscous drag or inertia forces are the dominant downward forces and the orifice diameter d_a only weakly influences the bubble volume since surface tension forces are negligible in the force balance (Fig. 5).

Considering the relation (6) for the drag coefficient C_d^*, an inertial parameter $\alpha = 11/16$ and a surface tension $\sigma = 0.06$ N/m, the force balance (5) then describes the bubble size increase with liquid viscosity and gas flow rate (Fig. 6). This model is quite predictive since the bubble detachment diameter is not very sensitive to the unknown parameters in the force balance: a 10% variation in the drag coefficient C_d^* or in the added fluid mass $\alpha\rho V$ mass leads respetively to a maximum error less than 2% or 1% in the bubble size.

No significant liquid depth dependence of bubble volume was further observed over the range 5 cm $< H <$ 15 cm (Fig. 7) because of the negligible influence of both pressure forces and large scale recirculation flow on bubble growth. The thickness $\delta \approx [\eta H/(\rho W_b)]^{1/2}$ of the viscous boundary layer (0.4 cm $< \delta <$ 3 cm with 0.043 Pa s $< \eta <$ 0.8 Pa s, 5 cm/s $< W_b <$ 40 cm/s, $\rho = 1250$ kg/m^3 and $H = 8$ cm) indeed remains short compared to the tank size (20 cm × 20 cm cross-section) and we may thus neglect the effect of large scale recirculation flow on bubble growth. In Section 5.3, we present some experiments showing the weak influence of recirculation flow on the process of bubble growth.

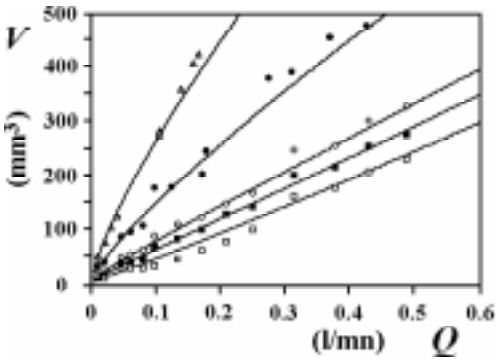

Fig. 6. Bubble volume V *versus* gas flow rate Q for nozzle diameter $d_a = 0.6$ mm. Experimental results for liquid viscosity $\eta = 43$ mPa s (□), $\eta = 105$ mPa s (■), $\eta = 164$ mPa s (○), $\eta = 475$ mPa s (●) and $\eta = 800$ mPa s (△). Solid lines are derived from equation (5) with $C_d^* = 24/Re + 1, \alpha = 11/16$ and $\sigma = 0.06$ N/m.

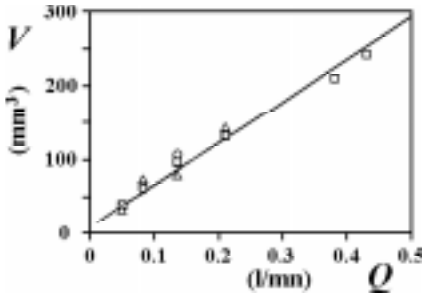

Fig. 7. Bubble volume V *versus* gas flow rate Q for nozzle diameter $d_a = 0.6$ mm and liquid viscosity $\eta = 164$ mPa s. Experimental results for liquid depth $H = 5$ cm (△), $H = 8$ cm (○) and $H = 12$ cm (□). Solid lines are derived from equation (5) with $C_d^* = 24/Re + 1, \alpha = 11/16$ and $\sigma = 0.06$ N/m.

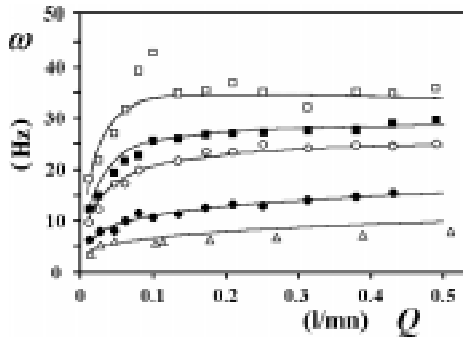

Fig. 8. Bubble frequency emission ω *versus* gas flow rate Q for nozzle diameter $d_a = 0.6$ mm. Experimental results for liquid viscosity $\eta = 43$ mPa s (□), $\eta = 105$ mPa s (■), $\eta = 164$ mPa s (○), $\eta = 475$ mPa s (●) and $\eta = 800$ mPa s (△). Solid lines are derived from equation (5) with $\omega = Q/V$, $C_d^* = 24/Re+1$, $\alpha = 11/16$ and $\sigma = 0.06$ N/m.

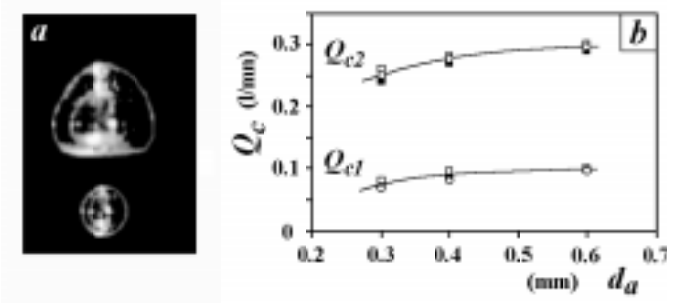

Fig. 9. a) Visualisation of pair bubble rise at the critical gas flow rate $Q_{c1} = 0.3$ l/mn in water glycerol solution of viscosity $\eta = 164$ mPa s ($d_a = 0.6$ mm). b) First and second critical gas flow rate Q_{c1} and Q_{c2} *versus* the nozzle diameter d_a for liquid viscosity $\eta = 43$ mPa s (□), $\eta = 105$ mPa s (■) and $\eta = 164$ mPa s (○).

The average bubble frequency emission ω derived from the analysis of the periodic signal pressure increases with gas flow rate and displays smaller values in high viscosity fluids. The bubble frequency estimated from $\omega = Q/V$ and equation (5) well agrees with experimental data as shown in Figure 8.

However, higher bubble frequencies are observed at the critical gas flow rate $Q_{c1} \approx 0.1$ l/mn (Fig. 8) for a Reynolds number $Re = W_b\, d\rho/\eta \approx 5$. Above the critical gas flow rate, image data and pressure signals show an abrupt transition resulting in larger bubbles with a smaller frequency. The transition is associated with the coalescence of closely interacting bubbles which first occurs near the liquid free surface where the spacing between bubbles is small and then extends to the nozzle region.

A second unstable regime was observed at the critical gas flow rate $Q_{c2} \approx 0.3$ l/mn in relation with pair bubble formation near the orifice (Fig. 9a). This alternative mode of bubble formation arises from the close interaction of a rapidly growing bubble with the previously detached bubble. Wake effects or gas exchange before the closure of the detached bubble may explain the non uniform size distribution. Above the critical gas flow rate Q_{c2}, bubble interference phenomena disappear resulting in larger bubbles of uniform size and lower emission frequency. The critical gas flow rates characterising the first and second transition regimes slightly increase with the nozzle diameter and display no significant dependence with fluid viscosity (Fig. 9b) since inertia forces determine the bubble motion.

We have observed other unstable regimes at higher gas flow rates ($Q > 0.5$ l/mn) which finally lead to the chaotic jetting regime. Under very high gas flow rate conditions, the gas momentum force exceeds the surface tension force then leading to the jetting regime for Weber number $We = d_a \rho_g W_g^2/\sigma > 1$ [15,28].

5.2 Bubble rise velocity

For air bubbles of diameter $d < 10$ mm and rising velocity $W_b < 0.5$ m/s in water-glycerol solutions (viscosity up to 800 mPa s), the Reynolds number $Re = W d\rho/\eta$ and the Eötvös number $E_0 = g\rho d^2/\sigma$ remain relatively small ($R_e < 10$ and $E_0 < 10$ with a surface tension $\sigma = 0.06$ N/m). Consequently, one can assume a nearly spherical shape for rising bubbles [9].

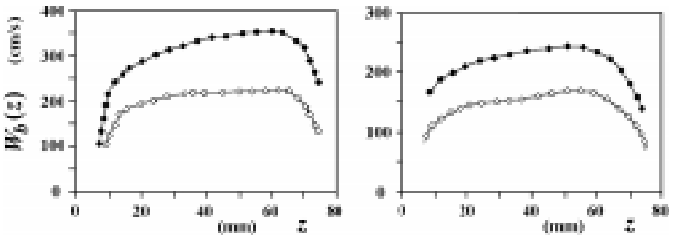

Fig. 10. Bubble rise velocity $W_b(z)$ along the vertical gas-liquid column for orifice diameter $d_a = 0.6$ mm, liquid depth $H = 8$ cm and gas flow rate $Q = 0.048$ l/mn (○) or $Q = 0.1$ l/mn (●). Experimental results for liquid viscosity $\eta = 43$ mPa s (left figure) and $\eta = 164$ mPa s (right figure).

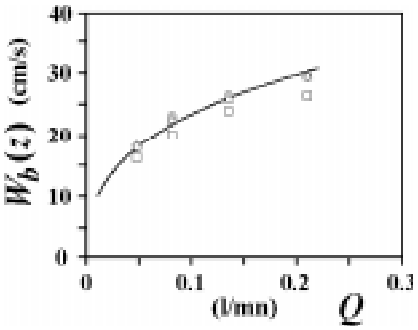

Fig. 11. Maximum bubble rise velocity W_b along the vertical gas-liquid column for orifice diameter $d_a = 0.6$ mm and liquid viscosity $\eta = 475$ mPa s. Experimental results for liquid depth $H = 5$ cm (□), $H = 8$ cm (△), and $H = 12$ cm (○). The solid line is derived from equations (5, 10) with $\varepsilon = Qd/W_bV$, $C_d = 16/Re + 1$, $\alpha = 11/16$ and $\sigma = 0.06$ N/m.

In the low gas flow rate regime ($Q < Q_{c1} \approx 0.1$ l/mn), bubbles generated in a stream indeed are spherical and uniform in size (Fig. 4a) since viscous forces are small compared with surface tension forces. For higher gas flow rates ($Q > 0.1$ l/mn), rising bubbles are larger and then become slightly deformed from the spherical shape with diameter-height ratio $1 < a/b < 1.1$ for 0.1 l/mn $< Q <$ 0.3 l/mn and $1.1 < a/b < 1.3$ for 0.3 l/mn $< Q <$ 0.5 l/mn.

From the measurement of the separation distance between corresponding bubbles in successive frames (Fig. 4c), we have determined the bubble rise velocity $W_b(z)$ along the gas-liquid column.

The analysis of image frames shows three stages in the bubble rise motion (Fig. 10). After an acceleration stage following the detachment from the nozzle, the bubble experiences a nearly uniform motion and a deceleration near the liquid surface. As shown in Figure 10, the bubble rise velocity undergoes significant variations along the gas-liquid column. Despite some acceleration of the bubbles in the stream, the maximum bubble velocity displays no significant variation with the liquid depth for $H \geq 8$ cm (Fig. 11) and can be considered as representative of the stationary rising velocity W_b. The constancy of the bubble rising velocity with liquid depth further results from the small thickness of the viscous boundary layer and the negligible influence of the large scale recirculation flow on the bubble stream dynamics.

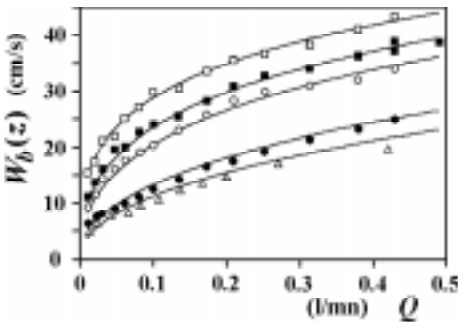

Fig. 12. Maximum bubble rise velocity W_b *versus* gas flow rate Q for nozzle diameter $d_a = 0.6$ mm. Experimental results for liquid viscosity $\eta = 43$ mPa s (□), $\eta = 105$ mPa s (■), $\eta = 164$ mPa s (○), $\eta = 475$ mPa s (●) and $\eta = 800$ mPa s (△). Solid lines are derived from equations (5, 10) with $\varepsilon = Qd/W_bV$, $C_d = 16/Re + 1$, $\alpha = 11/16$ and $\sigma = 0.06$ N/m.

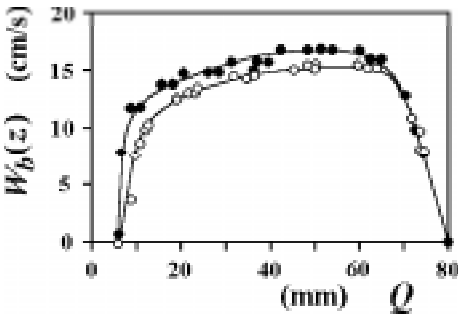

Fig. 13. Bubble rise velocity $W_b(z)$ along the vertical gas-liquid column for liquid viscosity $\eta = 164$ mPa s, gas flow rate $Q = 0.048$ l/mn and orifice diameter $d_a = 0.6$ mm with a circular ring of 3 cm diameter located near the emission orifice (●) or without screening ring (○).

Therefore, we may consider the bubble stream in an unbounded viscous fluid and use equation (10) to determine the bubble rising velocity. The variation of the maximum bubble rise velocity W_b with fluid viscosity and gas flow rate is well described by the non linear equations (5, 6, 10) over a wide range of Reynolds number (Fig. 12).

5.3 Influence of recirculation flow and adjacent bubble streams

We have studied the influence of the large scale recirculation flow on the bubble growth by screening the convective flows with a circular ring of 3 cm diameter located near the emission orifice (Fig. 14). The bubble rise velocity then decreases by about 8% (Fig. 13) since the circular ring screens the large scale reciruclation flow and then delays the detachment of the bubble. Despite a larger bubble volume, the increase separation distance between bubbles then results in a lower rise velocity. Davidson and Schuler [5] have reported a similar effect and a decrease of the bubbling frequency as the diameter of the screening ring was increased up to about 1.5 bubble diameter. However,

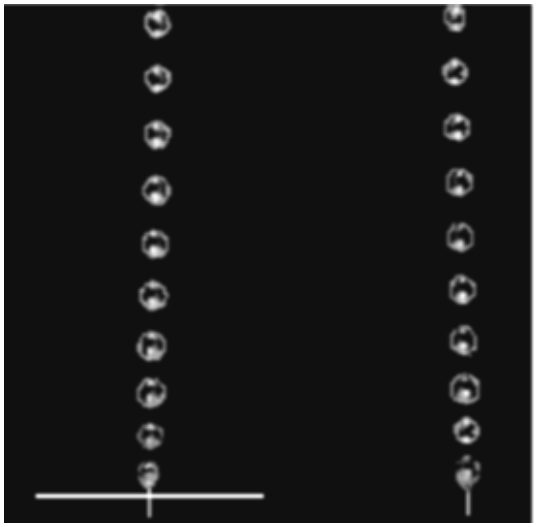

Fig. 14. Visualisation of interacting bubble streams distant from 5 cm for liquid viscosity $\eta = 43$ mPa s, gas flow rates $Q_1 = Q_2 = 0.05$ l/mn and orifice diameter $d_a = 0.6$ mm. Note the presence of a circular ring on the left emission orifice.

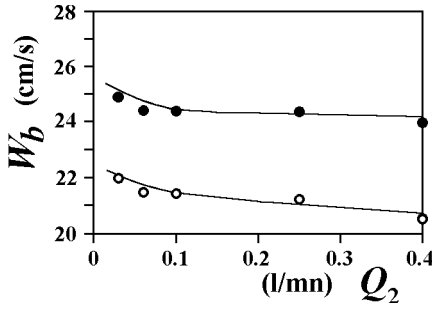

Fig. 15. Maximum bubble rise velocity emitted at constant air flow rate $Q_1 = 0.05$ l/mn from a first emission orifice with a circular ring (○) or without screening ring (●) *versus* the gas flow rate Q_2 through a second emission orifice distant from 5 cm. Liquid viscosity $\eta = 43$ mPa s and orifice diameter $d_a = 0.6$ mm.

the large scale recirculation flow near the nozzle weakly influences bubble growth and rise velocity.

We have also studied the interaction of two vertical bubble streams distant from 5 cm for liquid depth $H = 8$ cm, liquid viscosity $\eta = 43$ mPa s and gas flow rate $Q = 0.05$ l/mn (Fig. 14). Such a separation distance is larger than the thickness $\delta \approx [\eta H/(\rho W_b)]^{1/2} \approx 0.3$ cm of the viscous boundary layer and we may expect only small perturbation of the bubble streams.

An attraction between bubble streams which somewhat deviates the trajectory of bubbles is observed (Fig. 14). We have measured the size and rise velocity of bubbles generated in the first stream at constant flow rate ($Q_1 = 0.05$ l/mn) while increasing the gas flow rate Q_2 through the second nozzle. We have further investigated the effect of a circular ring located at the first emission orifice (Fig. 14). The small scale recirculation flow induced by the second bubble stream only weakly reduces the rising velocity of bubbles generated in the first stream (Fig. 15). The screening effect of the circular ring is more significant and induces a 12% decrease of the bubble rise velocity (Fig. 15). The ring screens the large scale recirculation flow near the emission orifice and the lower bubble rising velocity then results from the decrease of the gas volume fraction in the gas-liquid column. The rise motion of in-line interacting bubbles is more sensitive to hydrodynamic interactions between close bubbles than small variation in the bubble size.

6 Conclusion

The size of bubbles generated in a stable stream from a nozzle submerged in a viscous fluid was predicted by a semi empirical model based on a force balance just prior the bubble detachment from the nozzle. In the intermediate and high flow rate regime, surface tension forces are negligible and either viscous or inertia forces determines the bubble size. The wake force was neglected during stable bubble growth since the separation distance between bubbles always exceeds the bubble radius.

Unstable transition regimes were observed at high bubbling frequency leading to bubble coalescence near the liquid surface or pair formation bubble near the nozzle. Bubble coalescence occurs at critical gas flow rates resulting in larger bubbles of uniform size and lower emission frequency. The transition regimes display no significant dependence with fluid viscosity since inertia forces determine the bubble motion.

The rise velocity of stable bubble streams was estimated from an analogy with the settling rate of a long cylinder in an unbounded viscous fluid and from an energy balance on the gas-liquid column. The rise velocity of in-line interacting bubbles mainly depends on the bubble size and the gas volume fraction in the bubble stream. The net average bubbling force acting upward on the liquid near the bubble stream may be estimated from the liquid weight displaced by air bubbles within the stream.

The large scale recirculation flow was shown to have a weak influence on bubble size and rise velocity since the thickness of the boundary layer is small compared with the size of the tank. The screening of the recirculation flow with a circular ring located near the emission orifice induces only a small decrease of the bubble rise velocity. The constancy of the bubble size and rising velocity with liquid depth is a consequence of the negligible effect of the large scale recirculation flow on the bubble stream dynamics. The size and the rising velocity of bubbles are weakly affected by neighbouring bubble streams and small scale recirculation flows when separation distances are larger than the thickness of the viscous boundary layer.

References

1. W. Trier, *Glass furnaces, Design construction and operation* (the Society of Glass Tech., 1987).

2. R. Kumar, N.R. Kuloor, *The formation of bubble and drops*, Adv. in Chem. Eng. **8**, edited by T.B. Drew *et al.* (Academic Press, New York, 1970).
3. S. Ramakrishnan, R. Kumar, N.R. Kuloor, Chem. Eng. Sci. **24**, 731-749 (1969).
4. E.S. Gaddis, A. Vogelpohl, Chem. Eng. Sci. **41**, 97-105 (1986).
5. J.F. Davidson, B.O.G. Schuler, Trans. Inst. Chem. Eng. **38**, 144-154 (1960).
6. J.F. Davidson, B.O.G. Schuler, Trans. Inst. Chem. Eng. **38**, 335-342 (1960).
7. A.E. Wraith, Chem. Eng. Sci. **26**, 1659-1671 (1971).
8. A.K. Ghosh, J.J. Ulbrecht, Chem. Eng. Sci. **44**, 957-968 (1969).
9. R. Clift, J.R. Grace, M.F. Weber, Bubbles, *Drops and particles* (Academic Press, New York, 1978).
10. L.N. Milne-Thomson, *Theoretical hydrodynamics*, 3rd ed. (London, MacMillan & Co., Ltd, 1955).
11. Y. Kawase, J.J. Ulbrecht, Ind. Eng. Chem. Process Des. Dev. **20**, 636-645 (1981).
12. S.C. Chuang, V.W. Goldschmit, J. Basic Eng. 705-711 (1970).
13. K. Ruff, Chem. Eng. Technik. **44**, 1360-1372 (1972).
14. N. Rabiger, A. Vogelpohl, Ger. Chem. Eng. **5**, 314-320 (1982).
15. T. Miyahara, T. Haga, T. Takahashi, Int. Chem. Eng. **23**, 524-531 (1983).
16. T. Miyahara, T. Takahashi, Int. Chem. Eng. **25**, 146-148 (1985).
17. R.A.M. Al Hayes, R.H.S. Winterton, Int. J. Heat Mass Transfer. **24**, 223-231 (1981).
18. J.S. Hadamard, C.R. Acad. Sci. **152**, 1735-1738 (1911).
19. W. Rybczynski, Bull. Int. Acad. Sci. Cracovie A 40-46 (1911).
20. C. Alran, H. Angelino, Chem. Eng. Sci. **27**, 593-603 (1972).
21. J.F. Harper, Q.J. Mech. Appl. Math. **27**, 87-100 (1974).
22. G. Hestroni, S. Haber, Int. J. Multiphase flow **4**, 1-17 (1978).
23. D. Bhaga, M.E. Weber, Chem. Eng. Sci. **35**, 2467-2474 (1980).
24. L. Van Wijngaarden, J. Fluid Mech. **251**, 55-78 (1993).
25. J. Happel, H. Brenner, *Low Reynolds Number Hydrodynamics* (Prentice Hall Englewood clifts, New York, 1965).
26. P. Mills, P. Snabre, Rheol. Acta **26**, 105-108 (1988).
27. P. Snabre, P. Mills, Europhys. Lett. **25**, 651-656 (1994).
28. T. Miyahara, H. Terakado, T. Takahashi, J. Chem. Eng. Jpn **16**, 454-458 (1983).
29. K. Terasaka, H. Tsuge, Chem. Eng. Sci. **46**, 85-93 (1991).
30. P. Snabre, F. Magnifotcham, Eur. Phys. J. B **4**, 379-386 (1998).